PHYSICAL REVIEW B VOLUME 8, NUMBER 5 1 SEPTEMBER 1973

Electric and Dielectric Properties of Polycrystalline Yttrium Iron Garnet: Space-Charge-Limited Currents in an Inhomogeneous Solid

P. K. Larsen and R. Metselaar
Philips Research Laboratories, Eindhoven, The Netherlands
(Received 5 March 1973)

The dc conductivity of n-type polycrystalline yttrium iron garnet has been measured at temperatures near room temperature as a function of the applied voltage. At voltages below a critical value an Ohmic behavior is observed, while above this value we find $i \propto V^{\alpha}$, with $\alpha = 1.2-5.1$. ac conductivity and dielectric permittivity both show a large dispersion in the $10^{-3}-10^{5}$-Hz frequency range, e.g., a static value of the relative permittivity $\epsilon_s \approx 4000$ and a high-frequency value $\epsilon_\infty = 18$. The results are interpreted in terms of a two-layer model with well-conducting grains (e.g., $\sigma_{300\,K} \approx 7.2 \times 10^{-8}\ \Omega^{-1}\ cm^{-1}$) measuring 4 μm separated from each other by poorly conducting boundary layers (e.g., $\sigma_{300\,K} \approx 1.8 \times 10^{-15}\ \Omega^{-1}\ cm^{-1}$) of thickness 0.02 μm. At low voltages, conduction is determined by the boundary layer. At higher voltages, the current in the boundary layers is space-charge limited. A model is developed for space-charge-limited currents in an inhomogeneous solid of this kind. All experimental results can be explained qualitatively by this model. For one sample the measurements have been quantitatively analyzed. Good agreement with theory is found if we assume an exponential distribution of the density of states of the trapping centers in the boundary layers of the form $\mathfrak{N}_t(E) = N_t/kT_t\, e^{(E-E_c)/kT_t}$, with $N_t = 3.3 \times 10^{20}\ cm^{-3}$ and $T_t = 1110$ K. At 300 K, in the region of Ohmic conduction in the grain boundary layer ($V < 10$ V), the Fermi level of this layer is situated 0.88 eV below the conduction band; upon charge injection its position rises, for an externally applied voltage of 500 V, to about 0.63 eV below the conduction band. Annealing experiments at different oxygen pressures show that the poorly conducting boundary layers are regions which are reoxidized during cooling from the sintering temperature of 1430 °C to room temperature.

I. INTRODUCTION

A study of injected currents in insulators may provide valuable information on properties such as the density of states of the trapping centers which are present, and the drift mobilities of the free charge carriers. An extensive treatment of this subject is given in Ref. 1. If only one type of charge carrier is injected, the current will be space-charge limited. The steady-state current-voltage characteristic mostly follows a power law, the power being greater than or equal to 2. In polycrystalline samples of yttrium iron garnet (YIG), we observed a relationship between current and voltage following such a power law, but powers between 1 and 2 as well as greater than 2 were found. In contradiction to this, experiments on monocrystalline samples invariably yielded an Ohmic current-voltage dependence under comparable conditions. Though the sign of the Seebeck coefficient and the value of the activation energy of the conduction were the same for the monocrystalline and polycrystalline samples, the concentration and distribution of trapping centers can be widely different,[2] which might lead to the observed difference in the i-V characteristics. However, there is a dispersion of the dielectric properties of polycrystalline YIG samples which is not observed for monocrystalline YIG. Similar dispersion in the dielectric properties has been observed in a number of materials and is usually explained as being due to the effects of inhomogeneities.[3] In some of these materials non-Ohmic i-V relationships were explained as being due to the presence of potential barriers between the grains.[4,5] In this paper experiments on the dielectric and electrical properties of polycrystalline YIG will be described. The dielectric properties will be discussed on the basis of the Maxwell-Wagner layer model[6,7] in which the solid is assumed to be composed of layers of different conductance. Because the existing theories for non-Ohmic conduction in polycrystalline materials cannot explain our experimental results, we shall present a theory of space-charge-limited conduction (scl conduction) in an inhomogeneous solid. Our experimental results will be analyzed and discussed with the help of this theory.[8] Finally, the origin of the inhomogeneities and the influence of annealing treatments on the latter will be discussed.

II. EXPERIMENTAL

The samples investigated were cut from sintered pellets. High-purity yttrium-iron-garnet powder was made by using a spray-drying technique.[2] After hydrostatic pressing of the garnet powder, pellets were sintered for 4 h at 1430 °C in an oxygen atmosphere and cooled to room tem-

perature at a rate of 120 °C/h. The resulting material has a regular grain structure with a mean grain diameter of 4.5 μm (mean intercept length). Microscopic examination of a polished sample did not reveal any second phase. The results of a spectrochemical analysis of the sintered pellets are shown in Table I.

Some measurements were performed on materials of composition $Y_3Fe_{5-x}In_xO_{12}$ ($x \sim 0.05-0.25$) prepared by conventional ball milling.[9] Table I shows that the impurity content of this material is at least one order of magnitude higher than that of spray-dried samples. The average grain size of the indium-doped garnet is 25 μm.

The samples were usually of a thickness of 100–200 μm and had a surface area of 5–15 mm^2. Results will be presented for four samples, which can be regarded as typical. Samples 1 and 2 were different sections of one pellet, sintered from spray-dried powder. Sample 3 was made from another batch of spray-dried powder. Sample 4 was cut from a pellet sintered from ball-milled powder. Measurements were also performed on a pellet (of dimensions 8-mm diam and 2.75-mm height) made from the same starting material as used for samples 1 and 2.

Contacts were applied by rubbing an In-Ga mixture of eutectic composition on the surface. The surface was ground (preferably not polished) and cleaned, first in HCl and then in trichloroethylene, before the contacts were rubbed on. Measurements using a four-terminal method proved that reliable contacts were obtained in this way. Normally two contacts were placed on the sample and used for both dc conduction measurements and dielectric measurements.

dc conduction measurements were made using either the Keithley model-417 high-speed pico-ammeter or the Keithley model-640 electrometer. For measurements of the dielectric properties in the 20-Hz to 100-kHz frequency range a General Radio 1615A capacitance bridge was used. In the frequency range 0.001–10 Hz the ac current through the sample was measured and the in-phase and out-of-phase parts of this current with respect to the applied ac voltage then determined the conductive and capacitative parts of the current. In this case the Keithley model 417 was used for the current measurements.

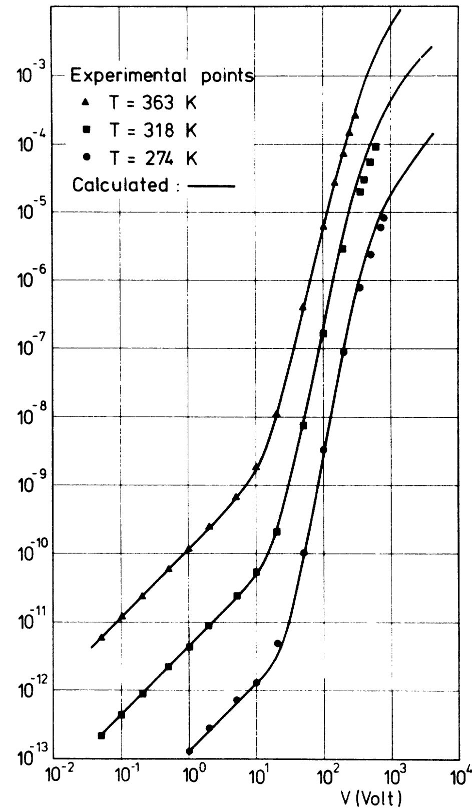

FIG. 1. dc current-voltage characteristic of undoped polycrystalline YIG (sample no. 1). ▲, experimental results at $T = 363$ K; ■, experimental results at $T = 318$ K; ●, experimental results at $T = 274$ K. Theoretical results (see Sec. V) are indicated by the lines. Electrodes on opposite sides of a 200-μm-thick sample. Electrode surface area 7.3 mm^2.

Measurements of the sign of the Seebeck coefficient at room temperature showed that all samples were n type.

III. EXPERIMENTAL RESULTS

A. dc Current-Voltage Characteristic

Figure 1 shows for sample 1 the dc thermal-equilibrium (dark) current as a function of the applied voltage for three temperatures. The calculated current-voltage characteristics shown by

TABLE I. Spectrochemical analysis of the impurity content of sintered polycrystalline samples prepared by different techniques.

Impurity concentration (mole %)	Mg	Si	Ti	Cr	Mn	Element Ni	Cu	Sn	Eu	Gd	Pt
spray dried	0.018	0.037	⋯	0.002	0.005	0.002	0.001	⋯	0.006	⋯	0.007
ball milled	0.180	0.250	0.080	0.100	0.620	0.200	0.030	0.020	⋯	0.040	0.007

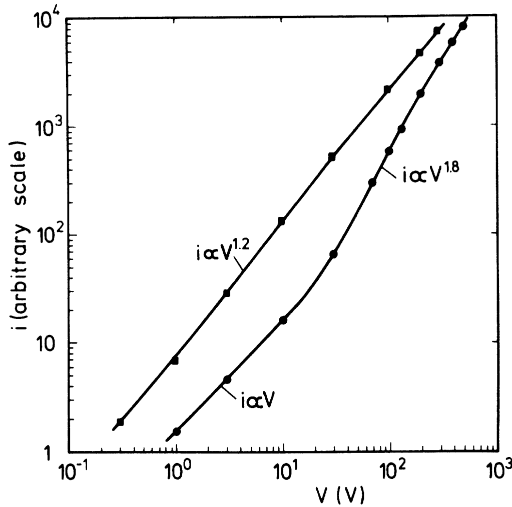

FIG. 2. dc current-voltage characteristics of undoped polycrystalline YIG (■, sample no. 3) and of a polycrystalline garnet of composition $Y_3Fe_{4.85}In_{0.15}O_{12}$ (●, sample no. 4).

the curves in this figure will be discussed in Sec. V. At low voltage, $V \lesssim 10$ V, an Ohmic relationship between current and voltage is observed. The resultant conductance G_s is found to be temperature activated with an activation energy of 0.7 eV. In the 10–30-V range, the slope in the log-log plot of the current-voltage characteristic changes from 1 below 10 V to a value of 4–5 above 30 V. Above 30 V, the current over approximately a voltage decade can be written

$$i = CV^{\alpha}, \quad (1)$$

where C and α are temperature-dependent constants. Values of α are listed in Table II. At the highest voltages a decrease in the slope of the i-V characteristic of Fig. 1 is observed. No indications of Joule heating of the sample were found.

To investigate the dependence of the current on the electrode distance L, the electrodes were placed on the same side of sample 2 (thickness 200 μm). The length of the electrodes was equal to the width of the sample. The current-voltage characteristic is similar to that of sample 1. In the voltage range where Eq. (1) holds we find a

TABLE II. Slopes α of the i-V characteristics of sample 1 at different temperatures, together with the corresponding characteristic temperatures T_t of the trap distribution.

T (K)	274	318	363
α	5.06	4.51	4.03
T_t(K)	1111	1116	1100

relation $i \propto L^{-\beta}$, where $\beta = 4.1 \pm 0.5$ at room temperature, while $\alpha = 2.6 \pm 0.3$.

However, for a number of samples a part of the current-voltage characteristic is given by $i \propto V^{\alpha}$, where $1 < \alpha < 2$. Figure 2 gives two examples of this. It should be noted that at the highest voltages a decrease in α is observed.

B. Dielectric Properties

High relative dielectric permittivities at low frequencies are found for our polycrystalline samples. A considerable variation in the dispersion is observed for the various samples. The static value ϵ_s of the apparent relative permittivity ϵ_r varies between 200 and 3×10^4. In this section we shall only present data for sample 1, but the results for sample 2 are quite similar.

In Fig. 3 the relative permittivity of sample 1 as a function of the frequency is shown. We verified that the measured dielectric properties were independent of the applied voltage in the voltage range used for these experiments. A temperature-dependent dispersion in ϵ is observed. At low frequencies a value ϵ_s of the order 4000 is found which is nearly temperature and frequency independent. At high frequencies the relative permittivity tends towards a temperature-independent value of approximately 18, which we shall denote ϵ_∞. Measurements on single crystals of undoped YIG give a nearly frequency-independent relative permittivity ϵ_i which is equal to ϵ_∞. We conclude on this basis that ϵ_∞ represents the true dielectric permittivity of the polycrystalline sample.

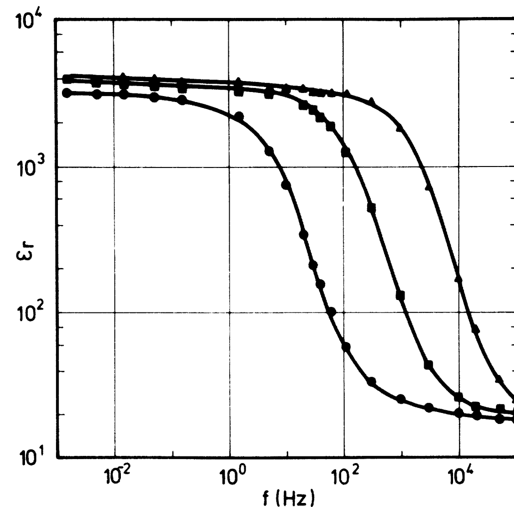

FIG. 3. Relative dielectric constant as a function of frequency for undoped polycrystalline YIG (sample no. 1). ▲, experimental results at $T = 363$ K; ■, experimental results at $T = 318$ K; ●, experimental results at $T = 274$ K. Electrode area and distance as indicated in Fig. 1.

TABLE III. Values of conductivities, relaxation times, and activation energies of sample 1 at 300 K.

	G_s	G_∞	τ_G	τ_ϵ
value at 300 K	$1.3\times10^{-12}\ \Omega^{-1}$	$2.9\times10^{-7}\ \Omega^{-1}$	1.1×10^{-3} sec	6.7×10^{-3} sec
activation energy (eV)	0.7	0.54	0.51	0.54

Figure 4 shows the ac conductance G of sample 1 as a function of the frequency. For low frequencies the conductance tends towards a limiting value G_s, which is the dc Ohmic conductance. The limiting value at high frequencies, G_∞, and G_s are indicated in the figure. In determining G_∞ we took into account the influence of a dielectric-loss peak situated in the MHz range. The values of G_s and G_∞ at 300 K and the activation energies are shown in Table III.

If the dispersion of the permittivity and the conductance is characterized by a single relaxation time τ, we have $\epsilon_r = \frac{1}{2}\epsilon_s$ and $G = \frac{1}{2}G_\infty$ for $\omega\tau = 1$, where ω is the angular frequency. Values of τ_ϵ and τ_G, determined, respectively, from $\epsilon = \epsilon(\omega)$ and $G = G(\omega)$, are found to be temperature activated, the values at 300 K and the activation energies are given in Table III. The activation energies of τ_ϵ and τ_G are in good agreement with each other and with that of G_∞. The difference in value between τ_ϵ and τ_G is thought to be due to a distribution of relaxation times. We shall further discuss the relaxation times in Sec. V.

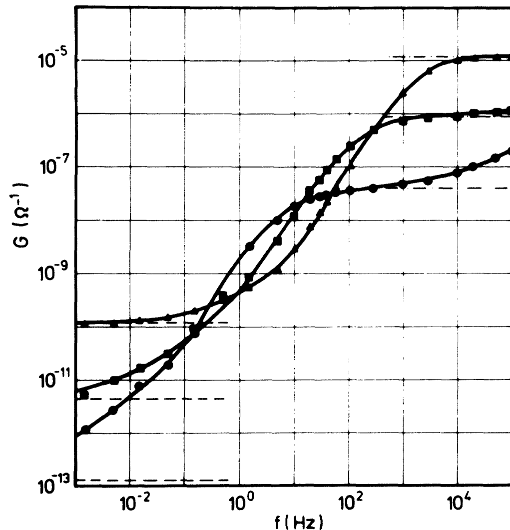

FIG. 4. Conductivity as a function of frequency for undoped polycrystalline YIG (sample no. 1). ▲, experimental results at $T = 363$ K; ■, experimental results at $T = 318$ K; ●, experimental results at $T = 274$ K. Electrode area and distance as indicated in Fig. 1. Dashed lines at the low-frequency side of the figure indicate the experimental values of the dc conductivity G_s. Dash-dot lines at the high-frequency side of the figure indicate the limiting values G_∞.

IV. DESCRIPTION OF AN INHOMOGENEOUS SOLID

A. Dielectric Dispersion: Maxwell-Wagner Layer Model

A qualitative description of high dielectric permittivities and low-frequency dispersion can be given by use of the Maxwell-Wagner layer model. The solid is assumed to be composed of well-conducting layers separated by poorly conducting layers. Applied to a polycrystalline material this corresponds to a situation in which layers of high resistivity exist between well-conducting grains. A detailed discussion has been given by Volger.[3] The most simple approximation is the two-layer model shown in Fig. 5.

The frequency dependence of the dielectric permittivity and the conductivity for a two-layer model was first described by Koops.[10] Referring to the discussion by Volger, we will only consider the case in which the conductance G_1 of the layers between the grains is much smaller than the conductance G_2 of the grains. We will further assume that the relative dielectric permittivity is the same for the two layers, i.e., $\epsilon_1 = \epsilon_2 = \epsilon_i$, and is independent of the frequency. With the aid of the equivalent RC circuit shown in Fig. 5, the apparent dielectric permittivity $\epsilon_r(\omega) = C(\omega)d/\epsilon_0$ and conductivity $\sigma(\omega) = G(\omega)d$ may be calculated. For $G_1 \ll G_2$ and $d_1 < d_2$, one finds

$$\epsilon_r(\omega) = \frac{\epsilon_s + \epsilon_\infty\omega^2\tau^2}{1+(\omega\tau)^2}\ , \tag{2a}$$

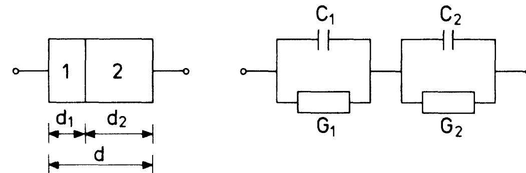

FIG. 5. Left-hand side: two-layer model for an inhomogeneous solid. A high-Ohmic layer 1 of thickness d_1, relative permittivity ϵ_1, and conductivity σ_1; and a low-Ohmic layer 2 of thickness d_2, relative permittivity ϵ_2, and conductivity σ_2. Right-hand side: equivalent RC circuit for a two-layer model of unit cross section. Capacities $C_1 = \epsilon_0\epsilon_1/d_1$ and $C_2 = \epsilon_0\epsilon_2/d_2$ in parallel with conductances $G_1 = \sigma_1/d_1$ and $G_2 = \sigma_2/d_2$.

$$\sigma(\omega)=\frac{\sigma_s+\sigma_\infty\omega^2\tau^2}{1+(\omega\tau)^2}\,, \qquad (2b)$$

where

$$\epsilon_s\approx\left(\frac{d}{d_1}\right)\epsilon_i,\quad \epsilon_\infty=\epsilon_i\,, \qquad (3a)$$

$$\sigma_s\approx\left(\frac{d}{d_1}\right)\sigma_1,\quad \sigma_\infty\approx\left(\frac{d_2}{d}\right)\sigma_2\,, \qquad (3b)$$

and

$$\tau\approx\epsilon_0\,\frac{\epsilon_s-\epsilon_\infty}{\sigma_\infty-\sigma_s}\;. \qquad (3c)$$

At frequencies $\omega \ll 1/\tau$, $\epsilon_r(\omega)$ is approximately equal to ϵ_s and it follows from Eq. (3a) that for $d_1 \ll d$ the apparent static permittivity will be very high. The temperature dependence of ϵ_i is generally small and it follows from Eq. (3a) that ϵ_s and ϵ_∞ are almost temperature independent. A further approximation of the relaxation time gives $\tau \approx \epsilon_0\epsilon_s/\sigma_\infty$, which means that the temperature dependence of τ is characterized by the temperature dependence of σ_2.

B. Origin of Non-Ohmic Current-Voltage Characteristics

Non-Ohmic i-V characteristics have been observed for a number of other polycrystalline materials.[4,5,8] In the models used by Heywang and by Krausse it is assumed that the grains are separated from each other by potential barriers ϕ, with a resistivity $\rho_s=\gamma\rho_v\,e^{\phi/kT}$. Here ρ_v is the volume resistivity of the grains and γ is a geometric constant. Since the potential barriers are assumed to be independent of each other, the voltage drop between the electrodes will vary linearly with the electrode distance L, i.e., $i \propto f(V/L)$, in opposition with our experimental results, which give $i \propto f_1(V)f_2(L)$. Moreover, application of this theory on our experimental results leads to internally inconsistent values of the height and width of the potential barriers.

For this reason we have looked for a different explanation of our results. The observed dc current-voltage relation and the dependence of the current on the electrode distance L is indicative of single carrier injection in a material in which traps distributed exponentially with respect to energy are present.[1] Let the trap distribution be given by

$$\mathfrak{N}_t(E)=(N_t/kT_t)e^{(E-E_c)/kT_t}\,, \qquad (4)$$

where $\mathfrak{N}_t(E)$ is the electron-trap density per unit energy, E is the energy, E_c is the energy of the conduction-band minimum, and N_t and T_t are constants characterizing the trap distribution. If $T_t \geq T$, the steady-state space-charge-limited current density $J_{\rm scl}$ for a homogeneous solid with a trap distribution given by Eq. (4) is

$$J_{\rm scl}=\mu N_c\,e^{1-l}\left(\frac{\epsilon_i\epsilon_0 l}{N_t(l+1)}\right)^l\left(\frac{2l+1}{l+1}\right)^{l+1}\frac{V^{l+1}}{L^{2l+1}}\,, \qquad (5)$$

where $l=T_t/T\geq 1$, N_c is the effective density of states in the conduction band, e is the elementary charge, μ is the drift mobility of the injected charge carriers (e.g., electrons), and L is the electrode distance. In the case $l<1$, Eq. (5) reduces to the shallow-trapping case,[1] in which $J_{\rm scl}\propto V^2/L^3$. Identifying the power α from Eq. (1) with $l+1$, T_t can be determined from $T_t=T(\alpha-1)$. In Table II, T_t as calculated from the measured values of α for sample 1, is tabulated. It is seen that the values of T_t determined from measurements at three different temperatures agree very well with each other.

Next, we consider the results for sample 2. We found $i\propto V^\alpha/L^\beta$, with $\alpha=2.6\pm0.3$ and $\beta=4.1\pm0.5$ at room temperature. For space-charge-limited currents, according to Eq. (5), α and β are related by $\alpha-1=\frac{1}{2}(\beta-1)$, in agreement with our experimental results. It seems therefore possible to identify the non-Ohmic part of the i-V characteristic with a space-charge-limited current. According to the dielectric measurements, we are dealing with inhomogeneous samples, while Eq. (5) was derived for a homogeneous solid. To investigate the consequences of the inhomogeneities, let us consider a structure consisting of two types of layers in series and assume that the current through the first type of layer (1) is space-charge limited, and through the other type of layer (2) is Ohmic. We further assume that the structure is of the form 1 2 1 2 1 .... The discussion will be restricted to steady-state conditions. We use the simplified theory for space-charge-limited currents, neglecting diffusion currents and using the boundary condition $\mathcal{E}=0$ at the cathode ($x=0$), where $\mathcal{E}=\mathcal{E}(x)$ is the electric field. The current density is given by

$$J=e\mu n_f(x)\,\mathcal{E}(x)\,, \qquad (6)$$

where $n_f(x)$ is the total number of free carriers (injected + thermal equilibrium). In layers of type 2 the injected-carrier concentration will be neglected, so $n_f(x)=n_{\rm eq}$ is independent of x in this layer. The electric field in type-1 layers is determined by Poisson's equation

$$\frac{d\mathcal{E}}{dx}=\frac{\rho}{\epsilon}\,, \qquad (7)$$

where $\rho(x)=-e\,[n_f(x)+n_{\rm tr}(x)]$ is the total charge, consisting of a free part $-en_f$ and a trapped part $-en_{\rm tr}$. The numbers of charge carriers n_f and $n_{\rm tr}$ are uniquely determined by the material properties and the temperature, i.e.,

$$n_f=f(n_{\rm tr})\,. \qquad (8)$$

The electric field $\mathcal{E}(x)$ in type-1 layers is determined by the relations (5)–(8) together with the boundary conditions. In addition to the condition $\mathcal{E}(0)=0$, we have the following conditions. Consider a type-2 layer situated between $x=x_n$ and $x=x_{n+1}$. The number of electrons in this layer is assumed to be constant and independent of x. This means $n_f(x_n^-)=n_f(x_{n+1}^+)$ and, because of Eq. (8), $\rho(x_n^-)=\rho(x_{n+1}^+)$. Let x_A be the distance from a position x in a type-1 layer to the cathode through type-1 layers only. We can then substitute $x=x_A$ in Eqs. (5)–(8) and, using the conditions $\mathcal{E}(0)=0$, the i-V characteristic can be calculated as for a homogeneous solid. The equivalent model for our inhomogeneous solid is therefore a two-layer model:

$$12121\ldots \propto 111\ldots \; 222\ldots \propto \sum_1 \sum_2 ,$$

where the summation means that the thickness of each layer in this model is found by adding the individual thicknesses of each type of layer.

The fact that we can treat the space-charge-limited current in layers of type 1 as for a homogeneous solid makes it possible to apply the theory for scl currents in homogeneous solids. For the trap distribution given by Eq. (4) the position-dependent quasi-Fermi-level $E_F(X)$ is given for steady-state injection by[1]

$$E_F(x)=E_c-kT_t \ln\left[\frac{(l+1)^2}{l(2l+1)}\,\frac{eN_tL^2}{\epsilon_0\epsilon_i V}\left(\frac{x}{L}\right)^{1/(l+1)}\right], \tag{9}$$

where x (>0) is the distance from the cathode at $x=0$. Equation (9) is valid for the case $n_f \gg n_{eq}$. If we evaluate $E_F(x)$ at the anode ($x=L$) (for our inhomogeneous solid, L equals the thickness of layer 1 in the two-layer model), only a small error is introduced, as shown by Lambert.[11]

C. Space-Charge-Limited Currents in a Two-Layer Model

Let us consider the equivalent model of Fig. 5 and assume that $G_1 \ll G_2$ and $d_1 \ll d$. According to Sec. IV A, the apparent static permittivity will then be high, which is in agreement with our experimental observations. Let V_1 and V_2 be the dc voltage drops across layers 1 and 2, respectively, and let

$$V=V_1+V_2 \tag{10}$$

be the externally applied voltage. If the currents through layers 1 and 2 are Ohmic, i.e., if

$$i_{\Omega 1}=G_1V_1 \tag{11a}$$

and

$$i_{\Omega 2}=G_2V_2, \tag{11b}$$

the voltage drop will take place mainly across the thin layer 1 ($V_1 \approx V$). This favors the observation of space-charge-limited currents in layer 1. We assume, therefore, that the total current i in the thin layer is composed of the Ohmic current $i_{\Omega 1}$ and a space-charge-limited current i_{scl}, while the current in layer 2 is Ohmic. The total current i is

$$i=i_{\Omega 1}+i_{\mathrm{scl}}=i_{\Omega 2}. \tag{12}$$

Assume

$$i_{\mathrm{scl}}=CV_1^\alpha , \tag{13}$$

where C and α (≥ 2) are voltage-independent constants [see Eq. (5)].

Equations (10)–(13) determine the i-V characteristic. We did a numerical calculation as shown in Fig. 6. The log-log plot of the i-V characteristic is S shaped with low- and high-current asymptotic values given by $i=G_1V$ and $i=G_2V$, respectively. The voltages V_{C1} and V_{C2} indicated in the figure are defined by

$$V=V_{C1} \quad \text{for } i_{\Omega 1}=i_{\mathrm{scl}} \tag{14a}$$

and

$$V=V_{C2} \quad \text{for } V_1=V_2. \tag{14b}$$

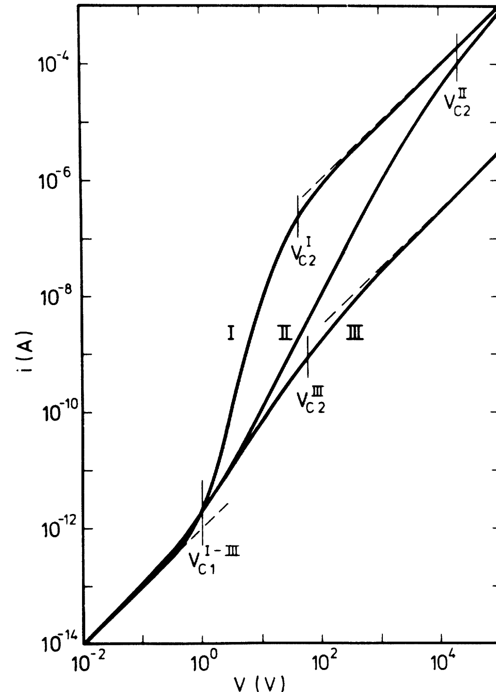

FIG. 6. i-V characteristic for a two-layer model of an inhomogeneous solid calculated under the following assumptions. Curve I: $G_1=10^{-12}\,\Omega^{-1}$, $G_2=10^{-8}\,\Omega^{-1}$, $\alpha=4$; Curve II: $G_1=10^{-12}\,\Omega^{-1}$, $G_2=10^{-8}\,\Omega^{-1}$, $\alpha=2$; Curve III: $G_1=10^{-12}\,\Omega^{-1}$, $G_2=3\times 10^{-11}\,\Omega^{-1}$, $\alpha=2$. V_{C1}, for which $i_{\Omega 1}=i_{\mathrm{scl}}$, is assumed in all cases to be 1 V.

The i-V characteristic consists of three parts:

(i) *Low-current Ohmic range*: $V < V_{C1}$, $V_2 \ll V$.

In this range $i_{scl} \ll i_{\Omega 1} \approx i \approx G_1 V$, and Ohm's law holds for voltages smaller than V_{C1}:

$$V_{C1} = (G_1/C)^{1/(\alpha-1)} . \tag{15}$$

(ii) scl-*current range*: $V_{C1} < V < V_{C2}$, $V_2 \ll V$.

The current through layer 1 is mainly space-charge limited: $i_{\Omega 1} \ll i_{scl} \approx i$. The current-voltage characteristic is given by (13), with $V_1 \approx V$ as long as $V_2 \ll V$, i.e., for $V \ll V_{C2}$, where

$$V_{C2} = 2(G_2/C)^{1/(\alpha-1)} . \tag{16}$$

(iii) *High-current Ohmic range*: $V_{C2} < V$, $V_1 \ll V$.

The current in this range is determined by the conductance of layer 2. The current through layer 1 is space-charge limited, but V_1 is relatively small and the current is approximately given by Eq. (11b), with $V_2 = V$.

The three ranges mentioned are indicated in Fig. 6. The following points are worth noting. The slope of the log-log plot of the i-V characteristic in part (ii) is equal to or *less* than the theoretical value α. By reducing G_2 in the example in Fig. 6, from the value of 10^{-8} to 3×10^{-11} Ω^{-1} the maximum slope for the curves with $\alpha = 2$ is actually reduced from 1.97 to 1.55. So slopes with nearly constant values between 1 and 2 may be observed over a fairly extensive voltage range, when G_1 and G_2 differ little.

When dielectric properties are measured, the presence of ac-scl currents will be observed in the form of a dependence of $\epsilon_r(\omega)$ and $G(\omega)$ on the applied ac voltage. To eliminate this factor a sufficiently low ac voltage should be used.

V. ANALYSIS AND DISCUSSION

A. Remarks on Layer Structure

The dispersion of the permittivity and the conductance observed for sample 1 can be ascribed to the presence of layers with different conductance, as follows from Sec. IV A. The high-frequency relative permittivity ϵ_∞ is, in accordance with Eq. (3a), found to be equal to the intrinsic permittivity ϵ_i, while the static permittivity $\epsilon_s \approx 200\,\epsilon_i$. Using Eq. (3a) we find $d_1 \approx d/200$ and $d_2 = d - d_1 \approx d$. A necessary condition for observing high static permittivities is that $G_1 \ll G_2$. In the temperature range studied, the ratio between the high-frequency conductance G_∞ and the static conductance G_s exceeds 10^5. With Eq. (3b) we find $G_1 = G_s$ and $G_2 = (d/d_2)^2 G_\infty \approx G_\infty$, and the condition is clearly fulfilled. A calculation of the relaxation time τ as given by Eq. (3c) yields $\tau = 4 \times 10^{-3}$ sec at 300 K. The activation energy of τ is that of G_2, viz., 0.54 eV. Table III contains relaxation times derived from the frequency dependence of ϵ and G. Fairly good agreement, as to both value and activation energy, with the relaxation time determined above is found. We conclude on the basis of this discussion that it seems definitely established that the sample is inhomogeneous, consisting of two types of layers of different conductance. The Maxwell-Wagner two-layer model describes the dielectric properties fairly accurately. We have shown that parts of the i-V characteristics for all samples were characterized by $i \propto V^\alpha$. For samples 1 and 2, $\alpha > 2$, while for samples 3 and 4, $\alpha = 1.2$ and 1.8, respectively (see Figs. 1 and 2). These samples, as the dielectric dispersion shows, are inhomogeneous, and the characteristics can be explained as space-charge-limited currents in an inhomogeneous layered structure. The model presented in Sec. IV gives a qualitative explanation of all our observations.

B. Quantitative Treatment of the i-V Characteristics

The i-V characteristic of sample 1 is described by the Eqs. (10)–(13). The constants G_1 and G_2 are here determined from the low-voltage Ohmic dc i-V characteristic and the high-frequency ac conductance, respectively. The space-charge-limited current given by Eq. (13) is described by Eq. (5) with the characteristic temperature $T_t = 1110$ K (see Table II). The thickness d_1 of layer 1 through which i_{scl} passes is shown to be $d/200 = 1$ μm. In order to calculate the constant C, knowledge of N_t and μN_c is also necessary.

N_t can be determined from the temperature dependence of the space-charge-limited current for constant voltage. In the voltage range in which the injected current is much greater than the thermal-equilibrium current, the quasi-Fermi level is approximately given by Eq. (9), with $x = L = d_1$ and $E_F = E_F(V)$. The number of free electrons corresponding to this quasi-Fermi level is given by $n_f = N_c \exp\{[E_F(V) - E_c]/kT\}$, and the current i_{scl} equals $e\mu n_f V$. Hall-effect measurements in Si-doped YIG have shown that the temperature dependence of the Hall mobility is small.[12] We shall henceforth assume that this is also the case for the drift mobility. We take the temperature dependence of N_c as $T^{3/2}$. With these assumptions we calculated the quasi-Fermi level as a function of the voltage from the observed temperature dependence of the current. The result is shown in Fig. 7. The dashed line in the figure was calculated from Eq. (9), with

$$N_t = 3.3 \times 10^{20} \text{ cm}^{-3} .$$

The fit with the experimental values is good. The electron trap distribution for layer 1 in the energy range $E_c - 0.85 \lesssim E \lesssim E_c - 0.6$ eV is thus given by Eq. (4), with $T_t = 1110$ K and N_t as given above.

In order to determine μN_c we note that all con-

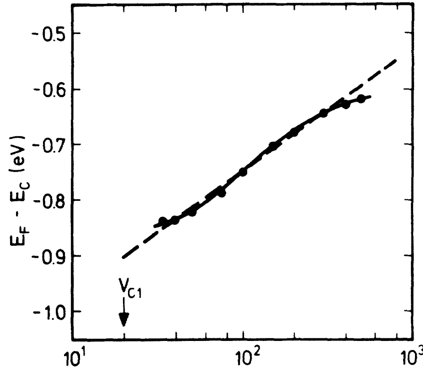

FIG. 7. Position of the quasi-Fermi level below the conduction band at 300 K as a function of an externally applied voltage. Points: experimental data for sample 1. Dashed line: calculated from Eq. (9), with $N_t = 3.3 \times 10^{20}$ cm^{-3}. V_{C1} denotes the voltage for which $i_{sc1} = i_{\Omega 1}$ at 300 K.

stants except μN_c in Eq. (5) are known. A comparison between measured and calculated current gives the value at $T = 300$ K:

$$\mu N_c = (6.0 \pm 0.9) \times 10^{18} \text{ (V sec cm)}^{-1}.$$

We can now calculate the constant C of Eq. (13) from Eq. (5) and determine the i-V characteristic. The result for the three temperatures 274, 318, and 363 K is shown in Fig. 1 for comparison with the experimental results. The over-all agreement is good. At high voltages the slope of both the theoretical and the experimental curves decreases, owing to the increase of V_2/V. The small discrepancy between the experimental and theoretical curves at high voltages can be ascribed to a less accurate determination of G_∞, to a limitation in the charge carrier injection, or to a change in the trap distribution.

The value of $N_c\mu$ given above is not representative for the bulk material. Monocrystalline Si-doped YIG (of composition $Y_3Fe_{4.91}Si_{0.09}O_{12}$), which is n type, has, at 300 K, a dc conductivity σ of 10^{-4} Ω^{-1}cm and an activation energy of 0.33 eV.[13] The activation energy depends only to a small extent on the donor (Si^{4+}) concentration and the almost-temperature-independent Hall mobility μ_H is 0.1 cm^2/V sec.[12] We will assume that the drift mobility $\mu_D = \mu_H$. The concentration n_{eq} of thermal equilibrium free carriers is given by[14]

$$n_{eq} \approx N_c[(N_D - N_A)/N_A]e^{-E_d/kT} . \qquad (17)$$

We have here assumed the presence of both donors and acceptors, with concentrations of N_D and N_A, respectively ($n_{eq} \ll N_A < N_D$). E_d is the donor ionization energy. The activation energy of the conductivity is equal to E_d if the mobility is temperature independent. The dominant acceptor in monocrystalline YIG grown from a PbO flux is Pb^{2+}. We estimate this concentration to be approximately 1×10^{20} cm^{-3},[15] while N_D for that single crystal is 3.8×10^{20} cm^{-3}. The conductivity is $\sigma = n_{eq} e \mu_D$ and, using Eq. (17), we find $N_c \approx 8 \times 10^{20}$ cm^{-3} and $\mu_D N_c \approx 8 \times 10^{19}$ (V sec cm)$^{-1}$ at 300 K.

We similarly analyzed our results for the well-conducting layers 2. Taking $E_d = 0.54$ eV and $(N_D - N_A)/N_A = 3$, we get $\mu N_c \approx 2 \times 10^{20}$ (V sec cm)$^{-1}$, which is fairly close to the result for the Si-doped YIG given above. The value of 6×10^{18} (V sec cm)$^{-1}$ for μN_c in layers 1 is about 10 times smaller than that of bulk material and we ascribe this to a lower mobility in the thin layers than in the grains, as there seems no reason to assume differences in the effective density of states between grains and grain boundary layers.

The Ohmic conductivity σ_s of layers 1 at 300 K is 1.8×10^{-15} Ω^{-1}cm^{-1}, and using $\mu N_c = 6 \times 10^{18}$ (V sec cm)$^{-1}$ we obtain $E_c - E_F = 0.88$ eV for the Fermi level when injection does not occur. This value agrees well with the results shown in Fig. 7 when it is realized that E_F is independent of the voltage V for $V < V_{C1}$. The differences in conductivity between the grains and the grain boundary layers ($\sigma_2/\sigma_1 \approx 4 \times 10^7$) can, thus, mainly be ascribed to a difference in the position of the Fermi level and, to a small extent, to a difference in mobility. In Sec. VI we shall discuss the origin of the difference in position of the Fermi levels.

VI. ANNEALING TREATMENTS

The experiments discussed above were performed on YIG samples with a low impurity content (spray dried) as well as a high impurity content (ball milled). In spite of the differences in impurity content between these two types of materials, the conductive and dielectric properties were fairly similar. The inhomogeneities responsible for the electrical behavior observed are therefore ascribed to intrinsic impurities.

At the sintering temperature of 1430 °C under 1 atm of oxygen pressure, yttrium iron garnet is slightly reduced. This reduction probably causes the formation of oxygen vacancies which can be compensated by ferrous ions.[2] We do not discuss the formation of interstitial cations, because we consider this not very likely. However, the treatment in the case of interstitials will be quite similar. During the cooling from the sintering temperature to room temperature a reoxidation occurs. The reoxidation depends on the oxygen diffusion rate, which decreases during the cooling. If the oxygen diffusion rate is greater along the grain boundaries than through the grains, as it is found for several materials,[16] the reoxidation of the grain boundaries will be greater than that of the grains. The grains will therefore have a higher conductivity than the grain boundaries. However,

in contradiction to our hypothesis, a single measurement of the O^{18} self-diffusion coefficient in YIG shows no difference between grains and grain boundaries.[17]

We tried to verify our hypothesis by means of annealing experiments. Samples were sintered in 1 atm of oxygen and then cooled under different conditions. Rapid cooling in 1 atm of O_2 produces a sample with $\epsilon_\infty = 17$ and $\epsilon_s = 8500$. Rapid cooling in a low oxygen partial pressure obtained by introducing nitrogen into the furnace produced a sample in which the static limit of the dielectric permittivity was not reached even at frequencies as low as 0.01 Hz. At this frequency ϵ was 3×10^4. The increase in ϵ can be due to a decrease of the thickness of the high-resistivity boundary layers, as is to be expected when the sample is cooled in a reducing atmosphere. Also, the number of boundary layers can be reduced. Moreover, the conductivity of the bulk material is slightly lower for the oxygen-cooled sample as compared with the samples cooled in nitrogen. We did not succeed in preventing the formation of boundary layers by quenching.

VII. THE NATURE OF TRAPPING CENTERS

In samples 1 and 2 we could describe our measurements by assuming an exponential trap distribution in the boundary layer. There are several independent indications pointing to the presence of continuous trap distributions in YIG, e.g., measurements of induced anisotropy,[18] ferromagnetic resonance,[19] light-induced changes in optical absorption,[20] and photo-induced changes in magnetic properties.[21] It would be interesting to know the nature and origin of these trapping centers.

From the analyses of the impurity concentration of the spray-dried samples, we find, neglecting intrinsic defects, $N_D - N_A \sim \frac{1}{4} N_D$. N_D is mainly determined by the Si concentration and if no intrinsic donors and acceptors were present, the Fermi level would be expected to lie about 0.3 eV (the ionization energy of Si-doped YIG) below E_c. However, we found $E_c - E_F = 0.88$ eV in Sec. V. On this basis the origin of the exponential trapping distribution should be sought in intrinsic defects. The influence of annealing treatments can be described by the presence of vacancies of oxygen and it is natural to relate the exponential trap distribution and the oxygen vacancies.

Oxygen vacancies may appear as neutral (V_0), singly positively charged ($V_0^{\bullet}$), and doubly positively charged ($V_0^{\bullet\bullet}$) in relation to the neutral lattice. (We use the Kröger-Vink notation.) The neutral and singly charged vacancies may be ionized and act as donors, but it is known from measurements on undoped YIG[2] and on Si-doped YIG[22] that part of the iron is present as Fe^{2+}. We therefore describe the oxygen vacancy in the form of donor complexes as

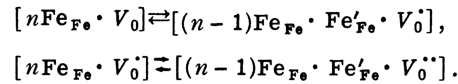

$$[n\mathrm{Fe_{Fe}} \cdot V_0] \rightleftarrows [(n-1)\mathrm{Fe_{Fe}} \cdot \mathrm{Fe'_{Fe}} \cdot V_0^{\bullet}],$$

$$[n\mathrm{Fe_{Fe}} \cdot V_0^{\bullet}] \rightleftarrows [(n-1)\mathrm{Fe_{Fe}} \cdot \mathrm{Fe'_{Fe}} \cdot V_0^{\bullet\bullet}].$$

Here $\mathrm{Fe_{Fe}}$ denotes an iron ion in its normal valence state (3+) on a normal lattice site. The notation for the donor complexes is intended to indicate that the electron moves in the coordination sphere of n iron ions surrounding the oxygen vacancies. When the donor complex is empty, we can describe the trapping of an electron by the reaction

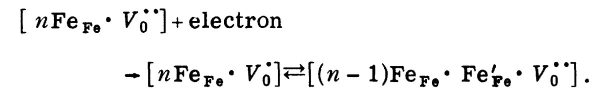

$$[n\mathrm{Fe_{Fe}} \cdot V_0^{\bullet\bullet}] + \text{electron} \rightarrow [n\mathrm{Fe_{Fe}} \cdot V_0^{\bullet}] \rightleftarrows [(n-1)\mathrm{Fe_{Fe}} \cdot \mathrm{Fe'_{Fe}} \cdot V_0^{\bullet\bullet}].$$

A quasicontinuous distribution arises with variation of the number n. This is equivalent to the picture of an $\mathrm{Fe'_{Fe}}$ ion at varying distances from the oxygen vacancy. The presence of neighboring complexes at varying distances in the lattice will also induce variations of the distance from the $\mathrm{Fe'_{Fe}}$ to the $V_0^{\bullet\bullet}$ within a given donor complex. The model presented in this article supports the qualitative models of Dillon *et al.*[20] and of Enz *et al*,[21] which were based on quite different experimental evidence. The energy distribution of traps described above is to be expected in both single crystals and polycrystalline material. Apart from this we have, in polycrystalline materials, regions of atomic disorder forming the grain boundaries, which can also give rise to a continuous trap distribution. Experimental evidence for this comes from measurements of, for instance, amorphous materials.[1]

SUMMARY

We have described the experimental results of measurements of the variation of the current as a function of an externally applied dc voltage on n-type polycrystalline YIG. At low voltages an Ohmic behavior is observed, while we find a power-law relationship $i = CV^{\alpha}$ at higher voltages. Dielectric measurements showed a strong dispersion of the permittivity and conductivity in the frequency range 10^{-3}–10^5 Hz. The dielectric behavior can be satisfactorily explained in terms of the Maxwell-Wagner model described in Sec. IV A.

We did not succeed to explain the dc current-voltage characteristic with the aid of the existing theories, i.e., with the assumption of potential barriers between the grains. Instead, we developed a theory of current injection in inhomogeneous solids.

In the non-Ohmic region the current is space-charge limited and largely determined by the number of free charge carriers in the boundary layers. For a quantitative description of one of our mea-

surements we assumed that the traps are distributed exponentially. We finally discussed the nature of the trapping centers. It was presumed that intrinsic defects, supposedly complexes consisting of an oxygen vacancy and a varying number of iron ions, are responsible for the continuous trap distribution observed.

We may summarize by saying that the observed current-voltage characteristic of polycrystalline YIG can be explained both qualitatively and quantatively in terms of injection of charge carriers into an inhomogeneous solid characterized by two layers with different conductivities. In particular, the theory would explain the experimentally observed occurrence of powers $\alpha < 2$ in the relation $i = CV^{\alpha}$, which is not possible according to the theory of scl currents in homogeneous solids.

ACKNOWLEDGMENTS

The authors wish to thank Professor G. H. Jonker for his valuable comments on this work, and P. Verburg for his assistance with the measurements.

[1]M. A. Lampert and P. Mark, *Current Injection in Solids* (Academic, New York, 1970).
[2]R. Metselaar and M. A. Huyberts, J. Phys. Chem. Solids (to be published).
[3]J. Volger, Progr. Semicond. 4, 207 (1960).
[4]W. Heywang, Solid State Electron. 3, 51 (1961); J. Am. Ceram. Soc. 47, 485 (1964).
[5]J. Krausse, Z. Angew. Phys. 27, 251 (1969).
[6]J. C. Maxwell, *Electricity and Magnetism* (Oxford U. P., Oxford, England, 1873), Vol. I, Sec. 328.
[7]K. W. Wagner, Ann. Phys. 40, 53 (1913).
[8]Nonlinear current-voltage characteristics in ZnO ceramics were ascribed to space-charge-limited currents by M. Matsuoka, Jap. J. Appl. Phys. 10, 736 (1971). However, measurements of the potential distribution across a sample show a linear relation between potential and distance [R. K. Eijnthoven (private communication)]. This result is incompatible with the interpretation given above.
[9]We are indebted to Dr. G. Winkler, Philips Forschungslabor., Hamburg, W.-Germany, for providing us with the ball-milled samples.
[10]C. G. Koops, Phys. Rev. 83, 121 (1951).
[11]M. A. Lampert, Phys. Rev. 103, 1648 (1956).
[12]D. C. Bullock and D. J. Epstein, Appl. Phys. Lett. 17, 199 (1970).
[13]R. E. Fontana, Jr. and D. J. Epstein, Mat. Res. Bull. 6, 959 (1971).
[14]J. S. Blakemore, *Semiconductor Statistics* (Pergamon, Oxford, 1962), p. 135.
[15]W. Tolksdorf (unpublished).
[16]Y. H. Oishi and W. D. Kingery, J. Chem. Phys. 33, 480 (1960); H. Hashimoto, M. Hama, and S. Shirasaki, J. Appl. Phys. 43, 4828 (1972); H. M. O'Bryan, Jr. and F. V. DiMarcello, J. Am. Ceram. Soc. 53, 413 (1970).
[17]A. E. Paladino, E. A. Maguire, Jr., and L. G. Rubin, J. Am. Ceram. Soc. 47, 280 (1964).
[18]R. P. Hunt, J. Appl. Phys. 38, 2826 (1967).
[19]T. S. Hartwick and J. Smit, J. Appl. Phys. 40, 3995 (1969).
[20]J. F. Dillon, Jr., S. M. Gyorgy, and J. P. Remeika, J. Phys. 32, C1-794 (1971).
[21]U. Enz, R. Metselaar, and P. J. Rijnierse, J. Phys. 32, C1-703 (1971).
[22]R. A. Lefever and A. B. Chase, J. Chem. Phys. 32, 1575 (1960).